Journal of Power Sources 196 (2011) 6567–6572

Contents lists available at ScienceDirect

Journal of Power Sources

journal homepage: www.elsevier.com/locate/jpowsour

Short communication

Cell/dendrite transition and electrochemical corrosion of Pb–Sb alloys for lead-acid battery applications

Wislei R. Osório[a,b,*], Daniel M. Rosa[c], Leandro C. Peixoto[b], Amauri Garcia[b]

[a] School of Applied Sciences / FCA, University of Campinas, UNICAMP, Campus Limeira, 1300, Pedro Zaccaria St., Jd. Sta Luiza, 13484-350 Limeira, SP, Brazil
[b] Department of Materials Engineering, University of Campinas, UNICAMP, PO Box 612, 13083-970 Campinas, SP, Brazil
[c] University of Brasilia, Faculty of Technology, UnB Campus Gama, PO Box 8114, 70910-90 Brasilia, DF, Brazil

ARTICLE INFO

Article history:
Received 31 January 2011
Accepted 24 March 2011
Available online 1 April 2011

Keywords:
Lead–antimony alloys
Lead-acid batteries
Cellular/dendritic transition
Electrochemical impedance spectroscopy

ABSTRACT

The aim of this article is focused on a comparative experimental study of the electrochemical feature of as-cast Pb–2.2 wt.% Sb alloy with cellular/dendritic transition for applications in the manufacturing of lead-acid battery parts. A water-cooled unidirectional solidification system is used to obtain the alloy samples. Electrochemical impedance spectroscopy (EIS) plots, potentiodynamic polarization curves and equivalent circuit analysis are used to evaluate corrosion resistance in a 0.5 M H_2SO_4 solution at 25 °C. The cellular Pb–2.2 wt.% Sb alloy is found to have a current density which is of about 3 times lower than that of the dendritic Pb–2.2 wt.% Sb alloy. The Pb–2.2 wt.% Sb alloy has lower current density than both the Pb–1 wt.% Sb and the Pb–6.6 wt.% Sb alloys evidencing its potential for application as positive grid material in lead-acid batteries. It is also verified that a conventional casting with low cooling rate of about 0.6 °C s^{-1} produces coarser cellular spacings which is more appropriate for the manufacturing of the Pb–2.2 wt.% Sb alloys grids due to its corresponding electrochemical behavior.

1. Introduction

Solidification interface morphologies have been widely investigated by many metallurgists, physicists and mathematicians for several decades, in which cellular/dendritic growth is one of the most complicated solidification patterns and is also the most prevalent form of crystallization [1]. The cellular and dendritic spacings are important microstructural parameters resulting from the solidification process, while it is well known that these spacings exercise a significant influence on the properties of castings [1]. The growth of regular cells is favored by low growth rate and low level of solute content during solidification of alloys, while dendrites growth is provided by high growth rate or high solute content [1,2].

Some studies existing in literature have focused on the characterization of cellular and dendritic growth of Pb–Sb alloys [3–11]. Osório et al. [12,13,15,16] and Peixoto et al. [14,17] reported that coarse cellular samples were associated with better corrosion resistance than fine cellular samples when considering experimental studies with Pb–Sb and Pb–Sn alloys subjected to corrosion tests in a 0.5 M H_2SO_4 solution. In previous report [12], it was indicated that a Pb–Sb alloy with Sb content high than 3 wt.% commonly provides a dendritic array. In this condition a fine dendritic spacing has higher corrosion resistance than coarse ones. On the other hand, it was also reported that conventional casting with low cooling rate will be more appropriate for the manufacturing of low Sb alloy grids (<3 wt.% Sb), since the resulting coarse cell morphology will have a higher electrochemical corrosion performance [12].

It was found that the improvement on the corrosion resistance depends on the cooling rate imposed during solidification which affects the morphology and the scale of the microstructure and the solute redistribution [8–17]. It is known that considerations of the grid-production capability, economic feasibility, metallurgical aspects and electrochemical behavior are important factors to the selection of appropriate levels of elements for the battery components. As reported by Rosa et al. [1], investigations characterizing the cellular/dendritic transition involving non-steady-state heat flow conditions are scarce in the literature. Despite its importance, since it encompasses the majority of industrial solidification processes, microstructural characterization of the cellular/dendritic transition and its effects on the corrosion resistance of a Pb–Sb alloy is focused in this present study. The effect of combined metallurgical features of as-cast Pb–2.2 wt.% Sb alloy considering cellular and dendritic arrays on the resulting electrochemical corrosion behavior in a 0.5 M H_2SO_4 solution at 25 °C is examined.

* Corresponding author at: University of Campinas, School of Applied Sciences, Pedro Zaccaria St., Jd. Sta Luiza, 13484-350 Limeira, São Paulo, Brazil. Tel.: +55 19 3521 3320; fax: +55 19 3289 3722.
E-mail address: wislei@fem.unicamp.br (W.R. Osório).

0378-7753/$ – see front matter © 2011 Elsevier B.V. All rights reserved.
doi:10.1016/j.jpowsour.2011.03.050

2. Experimental procedure

2.1. Specimens preparation

Commercially pure metals: Pb (99.90 wt.%) and Sb (99.35 wt.%) were used to prepare the as-cast Pb–2.2 wt.% Sb alloy. The mean impurities are: Fe (0.13%), Si (0.04%), Cu (0.018%), and other elements with concentration less than 50 ppm.

A water-cooled unidirectional solidification designed in such way that the heat was extracted only through the water-cooled bottom, promoting vertical upward directional solidification was used in the experiments. More details about of the solidification set-up can be obtained in previous articles [1,2,11–17]. Samples were sectioned from the center of the ingot, ground, polished and etched to reveal the macrostructure, as shown in Fig. 1. The microstructural characterization was carried out by using an optical microscopy associated with an image processing system Neophot 32 (Carl Zeiss, Esslingen, Germany) and Leica Quantimet 500 MC (Leica Imaging Systems Ltd., Cambridge, England) [1,2,11–17].

2.2. EIS and polarization tests

Electrochemical impedance spectroscopy (EIS) were carried out by using a 1 cm^2 circular area of ground (1200 grit SiC finish) sample surfaces, immersed in a stagnant and naturally aerated 500 cm^3 of a 0.5 M H_2SO_4 solution at 25 °C (±2) with pH 0.90 (±0.06). The measurements began after an initial delay of 30 min for the samples to reach a steady-state condition. The potential amplitude was set to 10 mV in open-circuit, peak-to-peak (AC signal), with 6 points per decade and the frequency range was set from 100 mHz to 100 kHz. The samples were further ground to a 1200 grit SiC finish, followed by distilled water washing (room temperature) and air drying before measurements. Potentiodynamic measurements were also carried out in the aforementioned solution at 25 °C (±2) using a potentiostat at the same positions where the EIS tests were carried out. Using an automatic data acquisition system, the potentiodynamic polarization curves were plotted and both corrosion rate and potential were estimated by Tafel plots by using both anodic and cathodic branches at a scan rate of 0.2 mV s^{-1} from −250/+250 mV (*vs.* SCE) at open-circuit. Duplicate tests for EIS and potentiodynamic polarization curves were carried out. In order to supply quantitative support for discussions of these experimental EIS results, an appropriate model (ZView®, Version 2.1b) for equivalent circuit quantification has also been used.

3. Results and discussion

3.1. Macro and microstructures

Fig. 1 shows typical directionally solidified casting macrostructure for Pb–2.2 wt.% alloy. The growth of columnar grains has prevailed along the entire casting length due to the water-cooled unidirectional system. The samples for the corrosion tests were collected at a midway position along the casting length (two different positions: P1 and P2), as also shown in a schematic representation in Fig. 1. Typical microstructures observed along (from the bottom of the casting) of both the transversal and longitudinal sections of the Pb–2.2 wt.% Sb alloy casting are shown in Fig. 2. The as-cast microstructure is consisted of a well-defined dendritic arrays from the bottom of the casting up to of about 30 mm, which is region with corresponding to the highest cooling rate from 20 ± 2 °C s^{-1} decreasing up to 6 ± 2 °C s^{-1}, as also previously reported [1]. It is important to remark that the used water-cooled system provides high cooling rate at the bottom of the casting and decreasing to top of the casting.

The dendritic/cellular transition occurred during the unidirectional growth of the Pb 2.2 wt.% Sb alloy casting at position between 30 ± 5 mm and 45 ± 5 mm from the bottom of the casting, corresponding with cooling rate ranged between 5.8 and 1.5 °C s^{-1}. In this range, lateral perturbations are observed, as reported by Rosa et al. [1]. Completely cellular arrays are observed after 45 ± 5 mm from the bottom surface up to the top of the casting, as schematically represented in Figs. 1 and 2. Detailed discussion concerning to the cellular/dendritic transition of the Pb–2.2 wt.% Sb alloy as a function of thermal solidification parameters were previously reported [1]. Rosa et al. [1] have demonstrated that there exists an experimental law ($\lambda = A\,(dT/dt)^{-0.55}$) which is independent of composition, characterizing the cooling rate dependence on cellular and primary dendritic spacing, where $A = 60$ represents the alloys undergoing a cellular growth and $A = 115$ can describe the dendritic growth. For cellular/dendritic transition of the Pb–2.2 wt.% Sb alloy, a sudden change on the multiplier has occurred [1]. They have also evidenced the experimental variation of both the cellular (λ_c) and dendritic primary spacings (λ_1) as a function of the liquidus isotherm velocity (V_L) and as a function of tip cooling rate (dT/dt) for the Pb–2.2 wt.% Sb alloy. Follow equations were obtained: $\lambda_c = 14\,(V_L)^{-1.1}$; $\lambda_1 = 27.5\,(V_L)^{-1.1}$ and $\lambda_c = 62.5\,(dT/dt)^{-0.55}$; $\lambda_1 = 140\,(dT/dt)^{-0.55}$ [1].

The obtained as-cast microstructures of the Pb–2.2 wt.% Sb alloy are constituted by a Pb-rich matrix (α-phase: solid solution of antimony in lead) with a eutectic mixture formation in the intercellular (P2) and interdendritic (P1) regions. Pb-rich matrix is represented by white regions with the interdendritic or intercellular regions depicted by dark regions.

In order to compare the resulting electrochemical corrosion behavior of the Pb–2.2 wt.% Sb alloy, same selected samples were chosen from casting length to attain the scale of the dendritic and cellular arrays.

3.2. EIS plots, equivalent circuit analysis and polarization measurements

Fig. 3 shows the Bode and Bode-phase plots representing the modulus of impedance ($|Z|$) and phase angle (θ) as a function of frequency (F). The experimental Bode-phase results indicate that at least two time constants can be associated with the corrosion kinetics of the matrix array (cellular or dendrite) and the intercellular or interdendritic regions. At a frequency range from 10^3 to 10^5 Hz, the first time constant is related with the electrochemical reaction between the Sb-rich phases (at intercellular or interdendritic regions) with the electrolyte. At low frequencies (between 10 and 70 Hz), the second time constant can be associated with the complex reactions among the Pb-rich matrix, adsorbed intermediates and electrolyte. A maximum $|Z|$ of about 300 and 500 Ω cm^2 at 0.1 Hz are observed for the Pb–2.2 wt.% Sb alloy at the positions P1 and P2, respectively. At frequency between 10 Hz and 10^3 Hz, a slope of the $|Z|$ *vs.* frequency suggests similar the nature and formation/evolution of the double layer. The maximum experimental phase angles (θ_{max}) at frequency of about 30 and 14 Hz for the dendritic (P1) and cellular (P2) Pb–2.2 wt.% Sb alloy samples were 47° and 59°, respectively.

Fig. 3(b) shows the experimental and simulated (Zview®) Nyquist plots of the Pb–2.2 wt.% Sb alloy samples. Nyquist plots reveal capacitive arcs at high frequencies (between 10^5 Hz and 1 Hz). It is clearly observed that the cellular microstructure has a higher capacitive arc (of about two times) than the dendritic microstructure sample. It is also evidenced that from about the 30 Hz to 100 kHz (which represent similar nature, formation and evolution of the double layer) these Nyquist plots are similar. From about 30 Hz to low frequency (representing the charge transfer and polarization resistances of both the Pb–Sb surface sample and

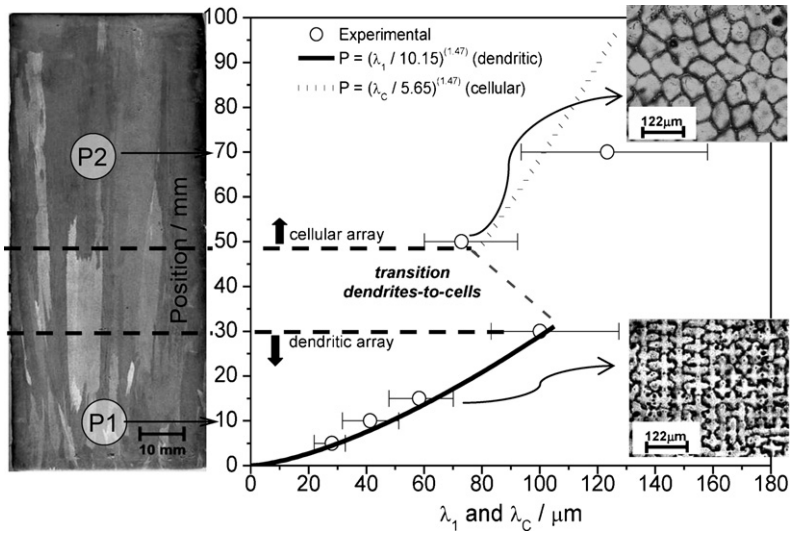

Fig. 1. Typical directionally solidified macrostructure of Pb–2.2 wt.% Sb alloy evidencing positions for corrosion tests and cellular and dendritic arrays as a function of the positions from the bottom of the casting.

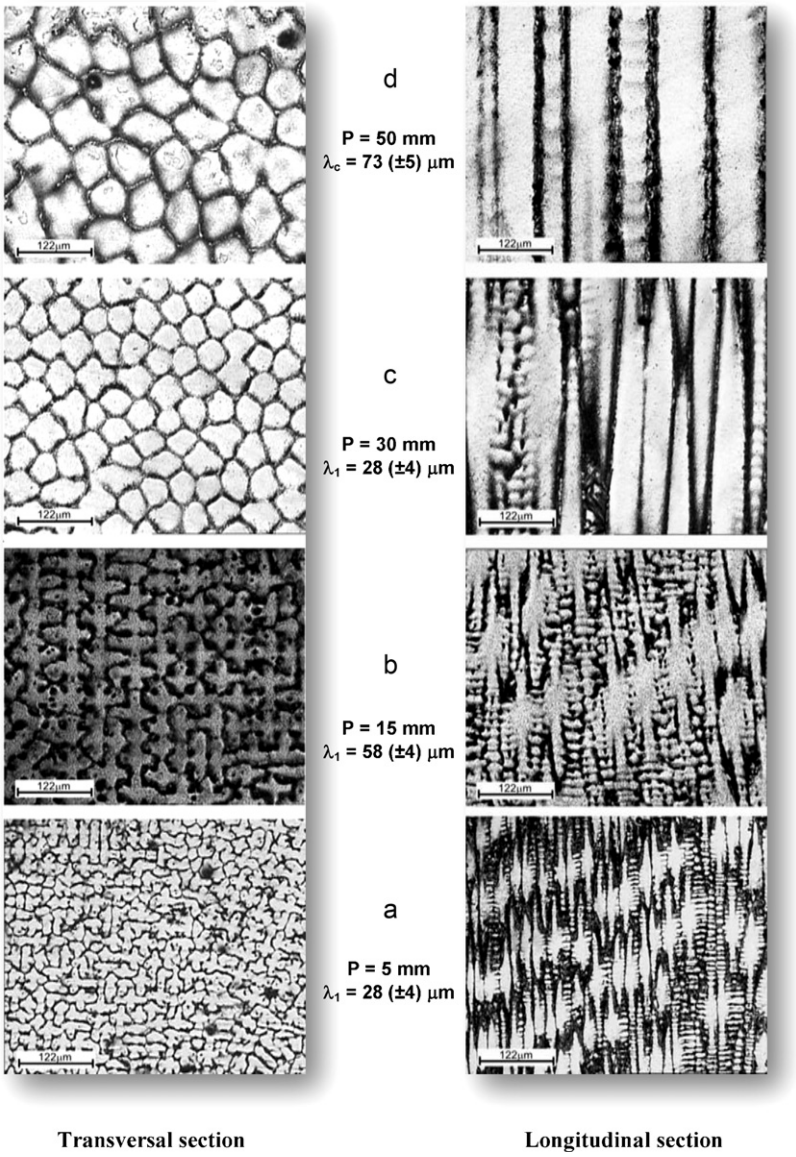

Fig. 2. Typical cellular and dendritic morphologies along the transversal and longitudinal sections for Pb–2.2 wt.% Sb alloy.

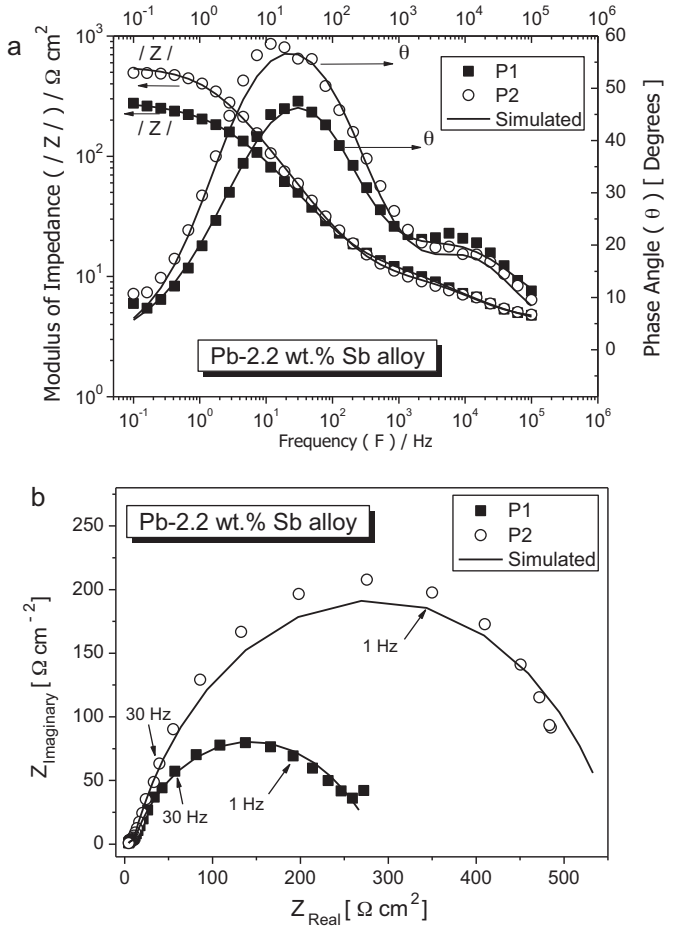

Fig. 3. (a) Experimental and simulated (ZView®) Bode and Bode-phase plots, and (b) Nyquist plots of the dendritic (P1) and cellular (P2) Pb–2.2 wt.% Sb alloy in a 0.5 M H_2SO_4 solution at 25 °C.

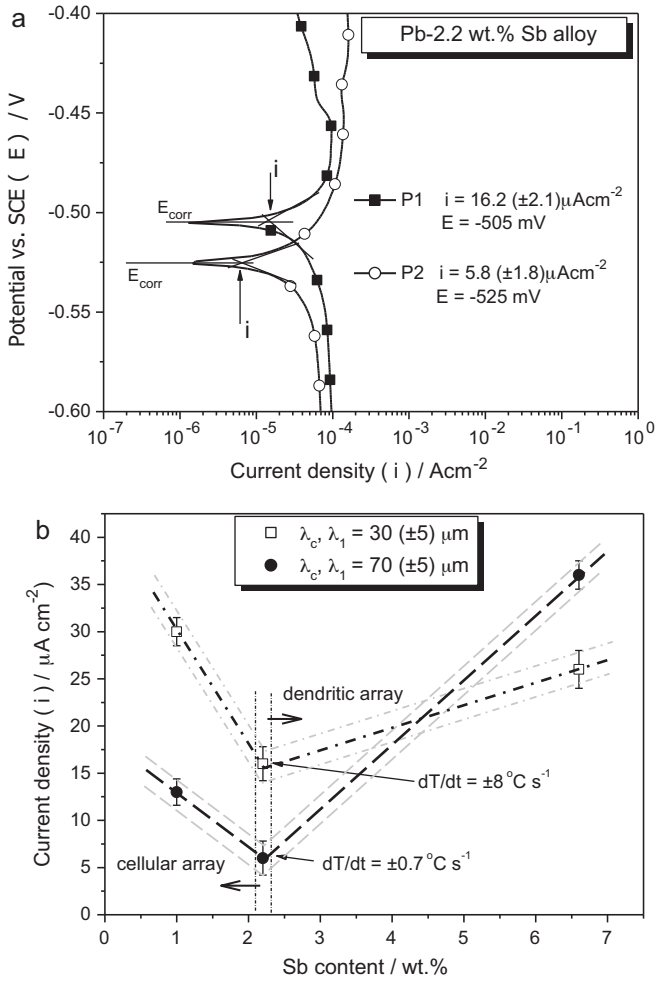

Fig. 4. (a) Experimental potentiodynamic polarization curves for Pb–2.2 wt.% Sb alloy samples in a 0.5 M H_2SO_4 solution at 25 °C and (b) the current density as a function of both the Sb content and the cellular and dendritic array.

adsorbed intermediates), the capacitive arcs are considerable different. These EIS plots provide clear indication that the cellular Pb–2.2 wt.% Sb alloy sample presents better electrochemical behavior than the dendritic Pb–2.2 wt.% Sb alloy sample.

In order to obtain the impedance parameters comparing the experimental EIS and simulated data using ZView® software, a complex $R_{el}(R_1(Z_{CPE(1)}(Z_{CPE(2)}R_2))$ equivalent circuit analysis has also been carried out, as previously proposed [11–22]. These impedance parameters are demonstrated in Table 1. The fitting quality was evaluated by chi-squared (χ^2) values of 10×10^{-4} and 38×10^{-4}. The interpretation of the physical elements of the proposed equivalent circuit is similar to those reported in previous studies [11–17]. Thus, R_{el} is the electrolyte resistance, R_1 is the charge transfer resistance and R_2 stands for a polarization resistance due to the participation of adsorbed intermediates. $Z_{CPE(1)}$ and $Z_{CPE(2)}$ denote the double layer capacitance and the capacitance associated with the polarization resistance R_2. The parameters n_1 and n_2 are correlated with the phase angle, varying between −1 and 1. The impedance of a constant phase element is defined as $Z_{CPE} = [C(j\omega)^n]^{-1}$ [8,11–17], where C is the capacitance; j is the current; ω is the frequency and $-1 \leq n \leq 1$. The value of n seems to be also associated with the non-uniform distribution of current as a result of roughness and surface defects [8,11–17]. It is observed that R_2 for both positions P1 and P2 is about 30 and 80 times higher than R_1, which indicates that R_2 has an important role on the electrochemical behavior, as shown in Table 1. The impedance parameters, $Z_{CPE(2)}$ and R_2 closely correspond to those of adsorbed intermediates (e.g. $PbSO_4$, PbOH and other). Although the dendritic Pb–Sb alloy sample (P1) has R_1 two (02) times higher than the cellular sample (P2), its corresponding capacitance $Z_{CPE(1)}$ is higher (of about 7 times, 436 μF cm^{-2}) than the cellular array (±60 μF cm^{-2}), which demonstrates better corrosion resistance associated with a high R_2 value (of about 2 times).

Table 1
Impedance parameters obtained by the ZView® software fitting experimental and simulated results for Pb–2.2 wt.% Sb alloy in a 0.5 M H_2SO_4 solution at 25 °C.

Parameters	Dendritic array	Cellular array
R_{el} (Ω cm^2)	3.6	4.3
$Z_{CPE(1)}$ (μF cm^{-2})	436 (±15)	60.5 (±3)
$Z_{CPE(2)}$ (μF cm^{-2})	213 (±3)	248 (±4)
n_1	0.55	0.74
n_2	0.79	0.78
R_1 (Ω cm^2)	12.6 (±0.3)	6.6 (±0.3)
R_2 (Ω cm^2)	273 (±3)	550 (±8)
χ^2	10×10^{-4}	38×10^{-4}

Fig. 4(a) shows potentiodynamic polarization curves (from −0.6 to −0.4 V *vs.* SCE) for the Pb–2.2 wt.% Sb alloy sample in a 0.5 M H_2SO_4 solution at 25 °C. The current density (i) was obtained from Tafel plots using both the cathodic and anodic branches of the polarization curves. A displacement of about 25 mV (SCE) in the corrosion potential of the dendritic Pb–2.2 wt.% Sb alloy sample (P1) is observed when compared with the cellular array sample (P2), which has a corresponding current density of about 6 ± 2 μA cm^{-2}.

Table 2
Microstructural morphology and corresponding parameters of the current density (i) and cooling rate (dT/dt) for the Pb–2.2 wt.% Sb alloy samples.

Parameters	Pb–1Sb		Pb–2.2Sb		Pb–6.6Sb	
Microstructure	Cellular	Cellular	Cellular	Dendritic	Dendritic	Dendritic
$\lambda_{c,1}/\mu m$	70 (±2)	30 (±5)	70 (±4)	30 (±3)	70 (±5)	30 (±6)
Cooling rate, $dT/dt/^{\circ}C\,s^{-1}$	0.7 (±0.1)	6 (±2)	0.6 (±0.1)	8 (±2)	0.2 (±0.1)	14 (±2.5)
Current density, $i/\mu A\,cm^{-2}$	13 (±3)	30 (±3	6 (±2)	16 (±2)	38 (±2)	26 (±3)

Considering the dendritic Pb–2.2 wt.% Sb alloy sample (P1), a current density of about $16 \pm 2\,\mu A\,cm^{-2}$ associated with a corrosion potential of about −505 mV (SCE) is observed.

3.3. Electrochemical parameters and microstructure comparison

These aforementioned experimental current density measurements associated with the EIS results induce that the cellular Pb–2.2 wt.% Sb alloy sample (coarse microstructure; $\lambda_c = \pm 70\,\mu m$; cooling rate ($dT/dt$): $\pm 8\,^{\circ}C\,s^{-1}$) has better electrochemical corrosion resistance than the dendritic Pb–2.2 wt.% Sb alloy sample (fine microstructure, $\lambda_c = \pm 30\,\mu m$; cooling rate ($dT/dt$): $\pm 8\,^{\circ}C\,s^{-1}$). It is known that during solidification of Pb–Sb alloys, antimony are segregated toward the cell boundaries and interdendritic regions [8,11–13]. For cellular and dendritic structures, galvanic cells are formed in the eutectic mixture at the cell boundaries and interdendritic regions, respectively. Previous studies [8,11–13] reported that the cell boundaries are regions of higher energy which is a result of distortions at the limits between adjacent cells during growth along the solidification process. It has also shown that coarser cellular structures tend to yield higher corrosion resistance than finer cellular structures for a dilute Pb–Sb alloy (±1 wt.% Sb) [8,11]. Similar tendency was also verified in previous studies reported by Peixoto et al. [14,17] and Osório et al. [11–13,15,16]. Such tendency of better corrosion resistance presented by coarser cells is associated with the reduction of cellular boundaries when compared with finer cells [8,11–17].

On the other hand, it was also concluded that finer dendritic array tends to yield higher corrosion resistances than coarser dendritic structure for a non-dilute Pb–Sb (Pb–6.6 wt.% Sb), as previously reported [12]. The dendritic array morphology has the antimony-rich regions located in the lamellar eutectic mixture. The Sb-rich lamellae will envelope the Pb-rich phase more efficiently for finer dendritic spacings due to the more extensive distribution of the eutectic mixture, and thus protecting the Pb-rich matrix [12].

The tendency of better electrochemical behavior exhibited by coarser cells of the Pb–2.2 wt.% Sb alloy is associated with the reduction of cellular boundaries. Although with a solute content ±2 times higher than the dilute Pb–1 wt.% Sb alloy, the Pb–2.2 wt.% Sb alloy can also be considered a dilute Pb–Sb alloy. The Pb–Sb phase diagram evidences a maximum solubility of antimony in lead of about 3.5 wt.% Sb and a eutectic composition lies about 11.2 wt.% Sb [12].

On the other hand, when a more extensively and finely distributed mixture of the Pb dendritic matrix and interdendritic regions (Sb-rich regions) are considered, the dendritic boundary increases the susceptibility to corrosion, similarly to that fine cellular microstructure of a dilute Pb–Sb alloy [8,12]. This occurrence is opposite to that previously observed for a more concentrated Pb–6.6 wt.% Sb alloy [12] which has presented a more homogeneously Sb-rich lamellae distributed in the eutectic mixture and the galvanic effect is diminished.

In order to understand the effect of the resulting microstructure morphology and Sb content on the experimental current density (i) for Pb–Sb alloys, previous results of a Pb–1 wt.% Sb [8] and Pb–6.6 wt.% Sb [12] alloys were compared with these presents results, as shown in Fig. 4(b). It can be seen that independent of the cell size (30 or 70 μm), the Pb–2.2 wt.% Sb alloy has lower current density than the Pb–1 wt.% Sb alloy. It is also evidenced that the resulting current density decreased with increasing the cellular spacing (of about 70 μm). The current density increases with increasing both the Sb content and dendritic spacing, when the dendritic morphological arrays of the Pb–2.2 and 6.6 wt.% Sb alloys are compared. It can also be concluded that independently of the cellular or dendritic arrays the Pb–2.2 wt.% Sb alloy sample has better corrosion resistance than both Pb–1 and 6.6 wt.% Sb alloys.

These experimental observations permit to conclude that the resulting microstructural morphology (which is strongly associated to both Sb content and cooling rate) has an important role on the electrochemical behavior of the Pb–Sb alloys.

Previous study [12] shows that the control of cooling rate can used as an alternative way to produce as-cast Pb–Sb grids for lead acid batteries with better corrosion behavior. It has been indicated that a solute content up to 3 wt.% Sb is conducive to a cellular morphology and that for alloys with antimony contents superior to 3 wt.%, a dendritic pattern is expected. In this context, in a conventional casting of the production of as-cast grids of Pb–Sb alloys, a low solute content alloy has to be associated with low cooling rate and coarse cell morphology in order to attain a better corrosion behavior. Considering a continuous casting process, a finer dendritic morphology will provide better corrosion behavior than coarser array.

Considering the present experimental, it is suggested that a conventional casting will be more appropriate for the manufacturing of the Pb–2.2 wt.% Sb alloy, since the resulting coarse cell morphology will have a higher corrosion resistance. On the other hand, high cooling rate (continuous casting) will produce finer dendritic spacings and higher current density is also be expected. Thus, preprogramming the solidification processing variables will be a considerable alternative way to produce as-cast Pb–Sb alloys battery grids by controlling the cooling rate during casting. Table 2 demonstrates the experimental current density (i), cooling rates (dT/dt) for the microstructure morphologies (cells and dendrites) of the Pb–1, 2.2 and 6.6 wt.% Sb alloys. It is evidenced that low cooling rate range (between 0.2 and $0.7\,^{\circ}C\,s^{-1}$) provides similar coarse microstructure arrays (±70 μm). The lowest current density is attained by the cellular Pb–2.2 wt.% Sb alloy. On the other hand, similar fine microstructure arrays (±30 μm) are obtained when cooling rate is between 6 and $14\,^{\circ}C\,s^{-1}$, which evidences a better corrosion resistance favoring the dendritic Pb–2.2 wt.% Sb alloy.

It is known that Pb–Sb alloys are widely used for the production of grids of positive electrodes of lead-acid batteries (between 1 and 6 wt.% Sb) [1,8,23,24]. These alloys are relatively strong and creep resistant and can be cast into rigid dimensionally stable grids, which are capable of resisting the stresses of the charge–discharge reactions [23,24]. It is evidenced that the antimony content of a Pb–Sb alloy can affect the microstructural pattern, mechanical properties, and electrochemical corrosion behavior [1]. Although a number of other Pb alloy systems can be considered for the production of lead-acid battery components, the manufacturers should consider the control of solidification processing variables (e.g. cooling rate and solute content) as reasonable and economical alternative in

order to improve the electrochemical behavior and other properties.

4. Conclusions

The present experimental investigations permit the following conclusions to be drawn:

- The EIS plots, potentiodynamic polarization curves and fitted equivalent circuit parameters have shown that both coarse and fine microstructure arrays of the Pb–2.2 wt.% Sb alloy tend to yield higher corrosion resistances than microstructures of the hypoeutectic Pb–1 and 6.6 wt.% Sb alloys. In the case of cellular morphology (between 30 and 40 mm from the bottom of the casting), such tendency of better corrosion resistance presented by coarser cells was attributed to the reduction of cellular boundaries, as similarly occurred in a dilute Pb–1 wt.% Sb alloy. On the other hand, the dendritic array morphology (attained from the bottom of the casting up to 30 mm) has a mixture of Pb-rich matrix and lamellar eutectic mixture at the interdendritic regions. These dendritic boundaries are more extensively distributed through Pb–Sb alloy lattice and susceptibility to corrosion is increased.
- Conventional casting processes with low cooling rates (of about $0.6\,^{\circ}C\,s^{-1}$) can produce cellular microstructure array ($\pm 70\,\mu m$) which will be more appropriate for the manufacturing of Pb–2.2 wt.% Sb alloy grids due to its corresponding electrochemical behavior. On the other hand, finer dendritic spacings ($\pm 30\,\mu m$) can also be produced when cooling rate of about $10\,^{\circ}C\,s^{-1}$ is applied in a continuous casting. In this operational condition, it was verified that the current density was increased of about three times ($\pm 16\,\mu A\,cm^{-2}$) when compared to coarse cellular spacing ($\pm 6\,\mu A\,cm^{-2}$).
- In order to produce the lead-acid battery components with better electrochemical corrosion behavior, the manufacturers of as-cast components should consider the control of solidification processing variables of dilute Pb–Sb alloys as an economical alternative.

Acknowledgements

The authors acknowledge the financial support provided by FAEPEX-UNICAMP, CNPq (The Brazilian Research Council), and FAPESP (The Scientific Research Foundation of the State of São Paulo, Brazil).

References

[1] D.M. Rosa, J.E. Spinelli, I.L. Ferreira, A. Garcia, Metall. Mater. Trans. A 39 (2008) 2161–2174.
[2] O.L. Rocha, C.A. Siqueira, A. Garcia, Mater. Sci. Eng. A 347 (2003) 59–69.
[3] L. Yu, G.L. Ding, J. Reye, S.N. Ojha, S.N. Tewari, Metall. Mater. Trans. A 30 (1999) 2463–2471.
[4] J. Hui, R. Tiwari, X. Wu, S.N. Tewari, R. Trivedi, Metall. Mater. Trans. A 33 (2002) 3499–3510.
[5] J. Chen, S.N. Tewari, G. Magadi, H.C. de Groh III, Metall. Mater. Trans. A 34A (2003) 2985–2990.
[6] D.M. Rosa, J.E. Spinelli, I.L. Ferreira, A. Garcia, J. Alloys Compd. 422 (2006) 227–238.
[7] B. Rezaei, S. Damiri, J. Solid State Electrochem. 9 (2005) 590–594.
[8] D.M. Rosa, J.E. Spinelli, W.R. Osório, A. Garcia, J. Power Sources 162 (2006) 696–705.
[9] M.A. Eshelman, V. Seetharaman, J.W. Trivedi, Acta Metall. 36 (1998) 1165–1174.
[10] X. Zhao, L. Liu, W. Zhang, Z. Yu, H. Fu, Mater. Chem. Phys. 125 (2011) 55–58.
[11] W.R. Osório, C.S.C. Aoki, A. Garcia, Mater. Sci. Forum 595–598 (2008) 851–859.
[12] W.R. Osório, D.M. Rosa, A. Garcia, J. Power Sources 175 (2008) 595–603.
[13] W.R. Osório, C. Aoki, A. Garcia, J. Power Sources 185 (2008) 1471–1477.
[14] L.C. Peixoto, W.R. Osório, A. Garcia, J. Power Sources 192 (2009) 724–729.
[15] W.R. Osório, L.C. Peixoto, A. Garcia, J. Power Sources 194 (2009) 1120–1127.
[16] W.R. Osório, L.C. Peixoto, A. Garcia, J. Power Sources 195 (2010) 1726–1730.
[17] L.C. Peixoto, W.R. Osório, A. Garcia, J. Power Sources 195 (2010) 621–630.
[18] W.R. Osório, L.R. Garcia, P.R. Goulart, A. Garcia, Mater. Chem. Phys. 106 (2007) 343.
[19] W.R. Osório, N. Cheung, L.C. Peixoto, A. Garcia, Int. J. Electrochem. Sci. 4 (2009) 820–831.
[20] J. Pan, D. Thierry, C. Leygraf, Electrochim. Acta 41 (1996) 1143.
[21] S. Gudic, J. Radosevic, M. Kliskic, Electrochim. Acta 47 (2002) 3009.
[22] F. Rosalbino, E. Angelini, D. Macciò, A. Saccone, S. Delfino, Electrochim. Acta 54 (2009) 1204.
[23] R.D. Prengaman, J. Power Sources 67 (1997) 267–278.
[24] T. Hirasawa, K. Sasaki, M. Taguchi, H. Kaneko, J. Power Sources 85 (2000) 44–48.